Advances in Science and Technology Research Journal

Advances in Science and Technology Research Journal 2023, 17(2), 173–180
https://doi.org/10.12913/22998624/161053
ISSN 2299–8624, License CC-BY 4.0

Received: 2023.01.16
Accepted: 2023.03.15
Published: 2023.04.01

Determination of Critical Damage Function Values of CW008A Copper and S355 Steel in Tensile and Torsion Tests

Patrycja Walczuk-Gągała[1], Zbigniew Pater[1], Łukasz Wójcik[1*], Konrad Lis[1]

[1] Department of Metal Forming, Faculty of Mechanical Engineering, Lublin University of Technology, ul. Nadbystrzycka 36, 20–618 Lublin, Poland

* Corresponding author's e-mail: l.wojcik@pollub.pl

ABSTRACT

The article addresses the problem of material fracture in metal forming processes. In the specialized literature as well as in the available technical catalogues, it is difficult to find the values of the damage functions according to the many available ductile fracture criteria for specific materials and specific shaping cases. Hence, experimental studies and numerical analyses were undertaken to determine the critical values of the damage function according to 9 ductile fracture criteria. The article undertakes to compare the values of damage functions obtained in classical calibration tests – tensile and torsion tests, under cold forming conditions. Two materials were selected for the study, i.e. CW008A copper and S355 steel. The presented research methodology includes experimental tests and numerical simulation carried out using Simufact. Forming v.15 software. The analysis of the obtained data made it possible to determine the value of damage using to various criteria, including the growth and coalescence of micro cracks (Rice&Tracey, Oyane, Argon), the initiation and development of ductile cracking in forming processes (Freudenthal, Cockroft-Latham, Brozzo, Oh) and using extended phenomenological models based on the history of stress triaxiality (Ayada) or the mean and equivalent stress (Zhan). The study showed that the value of the damage function is affected by the type of calibration test, the material grade and the geometry of the samples.

Keywords: material fracture, damage criterion, tensile test, torsion test, FEM.

INTRODUCTION

Metals and alloys fracture when subjected to a sufficiently high load. Cracking is the loss of material cohesion through separation or slippage and is considered to be the final stage in the deformation process of materials [1]. The cracking process depends on the type of material, its properties and deformation conditions (stress state, temperature, strain rate and environment) [2, 3]. Two different types of fracture can be distinguished among metallic materials [4]: brittle fracture, which is characterized by little or no plastic deformation before damage, and ductile fracture characterized by intense plastic deformation or emerging necking. The models used to predict fracture in the case of plastically shaped material are developed based on various damage criteria. The primary purpose of the criteria is to predict the location of crack occurrence and to determine the critical value of destruction. In the general case, the function describing the destruction of the microstructure of the material can take the relation:

$$C = \int_0^{\varepsilon_f} \Phi(\sigma) d\varepsilon$$

where: C – the critical value of the damage function,
ε_f – critical plastic strain at fracture,
$\Phi(\sigma)$ – function describing the effect of stress on the rate of void formation and coalescene.

Analysing the literature, Anderson [5] and Lemaitre et al [6] described ductile and brittle fracture, along with listing and describing individual

fracture criteria. Kraišnik et al [7] in an article provided an overview of the theoretical and experimental approaches used to define fracture criteria. In all of the aforementioned references, numerous group of ductile damage criteria based on the function Φ(σ) can be identified. Among the many damage criteria in ductile fracture, the criteria used in this study is listed in Table 1. In a general sense, the onset of failure is predicted when the ratio of the damage variable to the limit value of C_{gr} reaches a value of at least 1:

$$\frac{C}{C_{gr}} \geq 1$$

where: C_{gr} – the limit value of the damage function at the moment of fracture initiation.

The damage limit is obtained in calibration tests involving tension, compression and torsion of the specimens. The calibration methods used should reproduce or sufficiently approximate the test conditions to those of the real processes. Fischer et al [8] developed a damage indicator that can be calibrated by detailed inspection of the load displacement curve for a long and smooth specimen. Fuertes et al [9] determined that the damage value depends specifically on the geometry of the specimens. Kvačkaj et al [10] and Watanabe et al [11] studied specific cases of shaping – material, method, conditions – that allowed them to determine the value of the damage function. In addition, the results are valid only for forming cases characterized by a similar stress state to that occurring in the test. Factors that affect the results of calibration tests include: the type of the material's crystal lattice, structural state, conditions at the contact surface of the specimen with the holder, and the distribution of strain rates. There is insufficient information in the specialized literature regarding the critical damage values for a particular material as well as the conditions that must be met when applying the criteria. The most recent studies in the determination of damage function limits deal with specific shaping cases. Fuertes et al [9] in 2015 determined the damage function values according to the Cockcroft-Latham criterion for specimens made of AA5754 aluminium alloy with different geometries in compression test at 298.15 K. The author related the damage value obtained to the specimen geometry used. Jia et al [12] in 2018 tested AZ31B MG alloy at elevated temperature under uniaxial compression, the results obtained were evaluated by 6 ductile fracture criteria. The study showed that only the Freudenthal criterion is optimal for predicting surface cracks for the material under study. Pater et al [13] in 2019 determined the critical values of the damage function for R200 and 100Cr6 steels obtained by hot tensile testing. The study allowed the determination of critical values of damage functions for 7 ductile fracture criteria in the temperature range of 1273.15–1473.15 K.

Experimental studies and numerical analyses carried out for the article will allow the determination of critical damage function values according to several of the most commonly used ductile fracture criteria for the tested materials for a specific forming temperature using classical calibration tests. The obtained values will be applicable during the production of components subjected to ductile fracture.

Table 1. Selected damage functions used in ductile fracture analysis [5–7]

Criterion	Formula
Freudenthal	$\int_0^{\varepsilon_f(t)} \bar{\sigma} d\varepsilon \geq C_{FREU}$
Cockroft – Latham	$\int_0^{\varepsilon_f(t)} \sigma_{max} d\varepsilon \geq C_{CL}$
Oh	$\int_0^{\varepsilon_f(t)} \frac{\sigma_{max}}{\sigma_H} d\varepsilon \geq C_{OH}$
Brozzo et al.	$\int_0^{\varepsilon_f(t)} \frac{2\sigma_{max}}{3(\sigma_{max} - \sigma_H)} d\varepsilon \geq C_{BROZ}$
Ayada	$\int_0^{\varepsilon_f(t)} \frac{\sigma_H}{\bar{\sigma}} d\varepsilon \geq C_{AYAD}$
Oyane	$\int_0^{\varepsilon_f(t)} \left(1 + \frac{1}{A}\frac{\sigma_H}{\bar{\sigma}}\right) d\varepsilon \geq C_{OYAN}$
Zhan et al.	$\int_0^{\varepsilon_f(t)} (\sigma_{max} - \sigma_H) d\varepsilon \geq C_{ZHAN}$
Rice & Tracey	$\int_0^{\varepsilon_f(t)} exp\left(\frac{3}{2}\frac{\sigma_H}{\bar{\sigma}}\right) d\varepsilon \geq C_{RT}$
Argon et al.	$\int_0^{\varepsilon_f(t)} (\sigma_H + \sigma_{max}) d\varepsilon \geq C_{ARGO}$
where: $\bar{\sigma}$– effective stress [MPa], σ_{max} – maximal principal stress [MPa], σ_H – mean stress [MPa], A – material constant [-], ε_f – critical plastic strain at fracture [-]	

MATERIALS

Two materials were used for the tests, i.e. CW008A copper and S355 steel. The chemical compositions of the materials, are presented in Tables 2 and 3, respectively. The geometry and shape of the specimens used in the tests are shown in Figure 1. For tensile tests, three types of specimens were used – with different undercuts in

Table 2. Chemical composition of CW008A copper (weight percentage, %)

Cu	Bi	Pb	other
< 99.96	< 0.001	< 0.005	< 0.034

Table 3. Chemical composition of S355 steel (weight percentage, %)

C	Mn	Si	P	S	Cr	Ni	Al	Cu	Fe
0.2	1.5	0.2–0.5	≤ 0.04	≤ 0.04	≤ 0.3	≤ 0.3	≤ 0.02	≤ 0.03	others

the centre to study how the stress state affects the cracking of the material.

METHODS – EXPERIMENTAL TESTS

In order to determine the critical values of damage function, a tensile and torsion test were carried out. The moving tool in tensile test moved at a velocity of 5 mm/min, in the torsion test was equal 500 °/min. The tests were carried out at 293.15 K. Experimental tests were conducted until the specimens broke. The INSTRON 1000HDX tensile testing machine was used to break the specimens for tensile testing, and the WP510 torsion testing machine was used for torsion testing.

The tensile and torsion specimens for both tested materials broke during the experiment (Figures 2 and 3). In the case of both tested materials, in the tensile test, the fracture occurred in the center of the necking, in the expected location. In the type 1 and type 2 specimens for CW008A copper and S355 steel, a crack occurred as a result of narrowing, and a characteristic neck appeared. During the torsion tests in both tested materials, the specimens broke as a result of shear stress. The characteristic twisting of the material's fibers can be seen on the lateral surface of the samples.

By conducting experimental tests and numerical analyses, the distributions of forming load and torsional moment were recorded (Figures 4 and 5). The magnitudes of the data obtained from the experiments and from the numerical analyses shows that the results of calculations and experiments are very consistent in terms of quality. Additional friction was not taken into account during the numerical analyses, hence the higher values of forces and moments can be seen. Comparative analysis of the obtained quantities, allowed us to conclude that tensile and torsion tests were modeled correctly. From the analysis of figure 4, it can be read that the smaller the undercut radius, the higher the maximum load. The value of the load decreases after the appearance of the specimen's

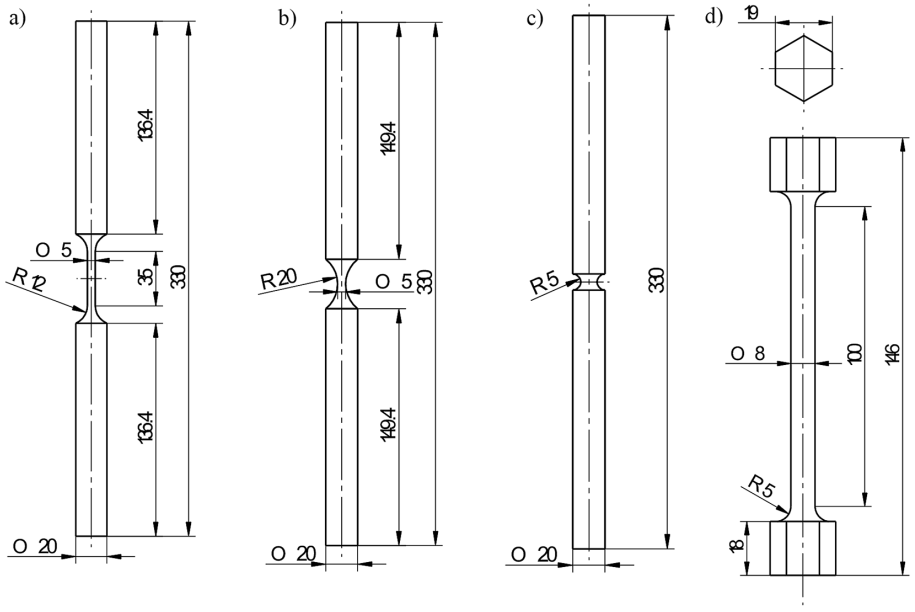

Figure 1. Samples used for calibration tests: (a) tensile test – type 1, (b) tensile test – type 2, (c) tensile test – type 3, (d) torsion test

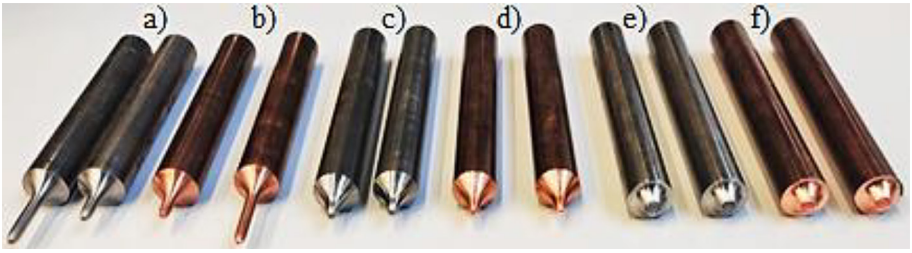

Figure 2. Elements after the tensile test: (a) S355 steel – type 1, (b) CW008A copper – type 1, (c) S355 steel – type 2, (d) CW008A copper – type 2, (e) S355 steel – type 3, (f) CW008A copper – type 3

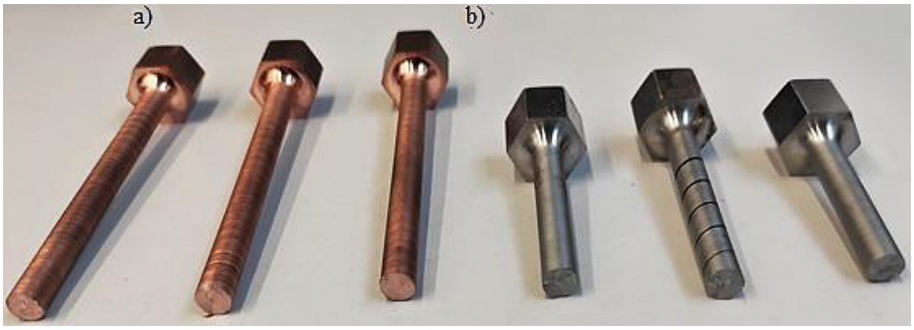

Figure 3. Elements after the torsion test: (a) CW008A copper, (b) S355 steel

necking. The distribution of forces for specimens type 1 and type 2 has a similar course – the fracture occurs at the same moment and at a relatively similar load. The force values recorded for S355 steel are about two times higher than the force values for CW008A copper. In the case of torsion of specimens made of CW008A copper, fracture occurred after 22 full rotations of the specimen. The S355 steel specimen broke after 8 rotations. The torsional torque values for CW008A copper are almost twice as low as for S355 steel.

NUMERICAL ANALYSIS

Numerical analysis of the calibration tests for both test materials was carried out in the Simufact.Forming v.15 software environment, in order to determine the critical values of the damage function. Figure 6 shows the geometric models of each test, which are identical to the tests carried out under laboratory conditions. For the numerical analysis of tensile tests, tool geometry was modified using Solid Edge software, i.e. the jaw chucks of the testing machine were simulated as a set of two rings. After modification, the speed of the moving ring was 5 mm/min, while the bottom ring remained stationary. In the torsion test, one of the grips moved at a speed of 500 °/min. The nether tool was fixed. On the basis of our own plastometric tests, the friction factor and material models described by the following equations were determined:

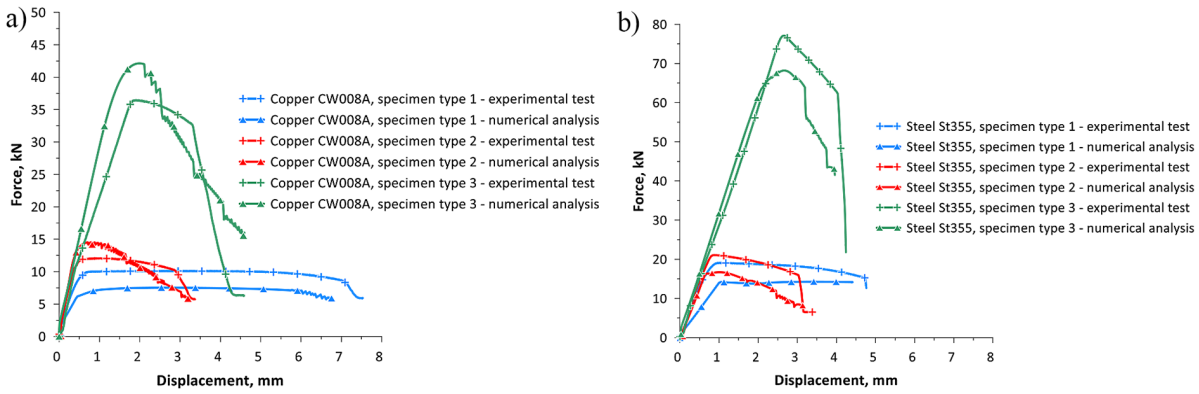

Figure 4. Distributions of forming load experimentally determined and numerical calculated in tests of tensile

- in tensile test for CW008A copper:

$$\sigma_p = 665.0 \cdot \varepsilon^{0.34} \quad (1)$$

- in torsion test for CW008A copper:

$$\sigma_p = 299.679 \cdot \varepsilon^{0.189} \quad (2)$$

- in tensile test for S355 steel:

$$\sigma_p = 1785.5 \cdot \varepsilon^{0.368} \quad (3)$$

- in torsion test for S355 steel:

$$\sigma_p = 937.982 \cdot \varepsilon^{0.164} \quad (4)$$

where: σ_p – flow stress [MPa]

Other data adopted for numerical analyses are shown in Table 4.

For the creation of the numerical grid, tetmesh elements of the size were used: a) tension – 2.5 mm, b) torsion – 1.0 mm. In an effort to quantitatively evaluate the issue under study along the radius at the midpoint of the test section (tensile and torsion), sensors spaced every 0.5 mm were introduced, where the parameters needed to determine the damage function were recorded (Figure 7). Numerical simulations allowed the determination of stress and dimensionless distributions damage functions for both materials (Figure 8–11).

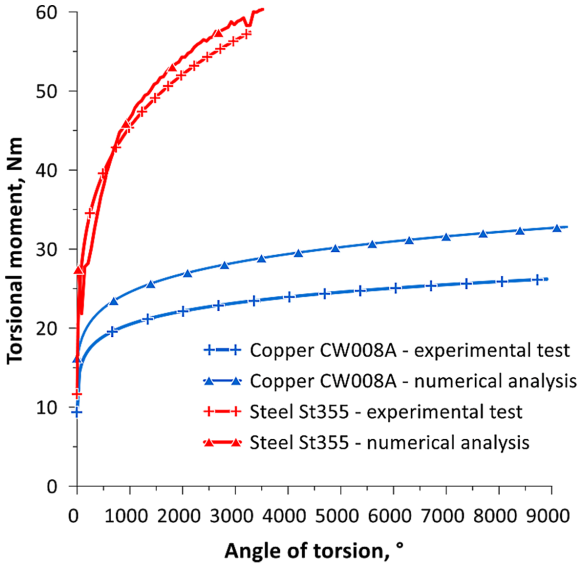

Figure 5. Distributions of torsional moment experimentally determined and numerical calculated in tests of torsion for CW008A copper and S355 steel

For the materials tested in the tensile test for all types of specimens, the values of stress and dimensionless damage functions in the cross-section show a linear distribution – at each point tested, there was a constant value at the location of the resulting necking. On the other hand, the values obtained in the torsion test show the lowest value at the point located in the centre of the specimen and increase as the lateral surfaces are approached.

The numerical analysis and experimental tests carried out made it possible to determine

Table 4. Numerical analysis parameters for tensile and torsion test of CW008A cooper and S355 steel

Parameter	Value
Friction factor [-]	CW008A copper – 0.43 S355 steel – 0.4
Temperature of specimens [K]	293.15
Heat transfer coefficient for specimen-tool [W/m²·K]	20000

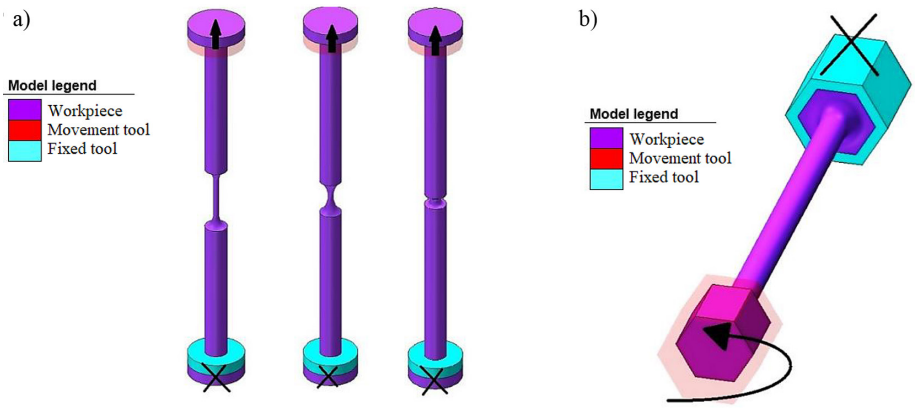

Figure 6. Geometric models of: (a) tensile test, (b) torsion test

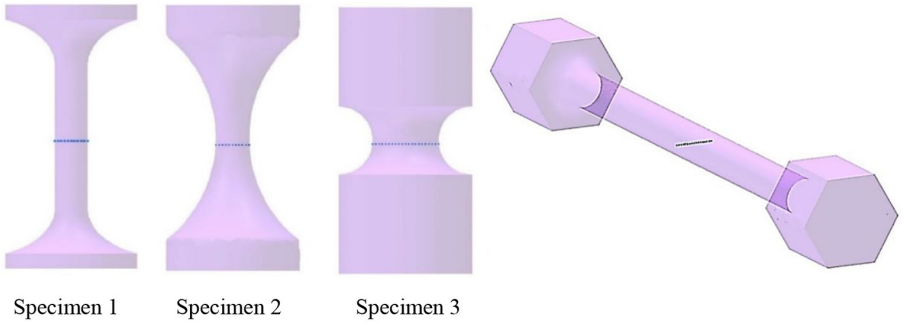

Figure 7. Arrangement of sensors in the axis of the specimen in: a) tensile, b) torsion tests; used to track parameters describing the state of stress and strain, the presented example applies to both materials of the specimens used for testing

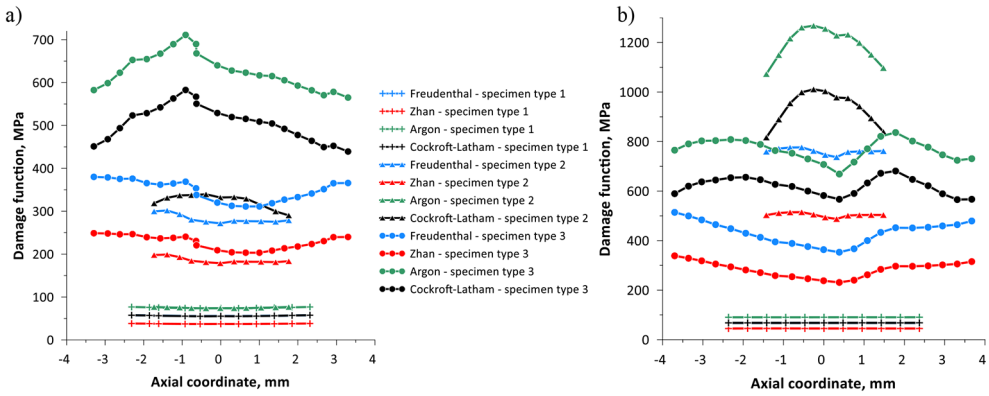

Figure 8. Distribution of stress damage functions for: a) CW008A copper, b) S355 steel, in the tensile test

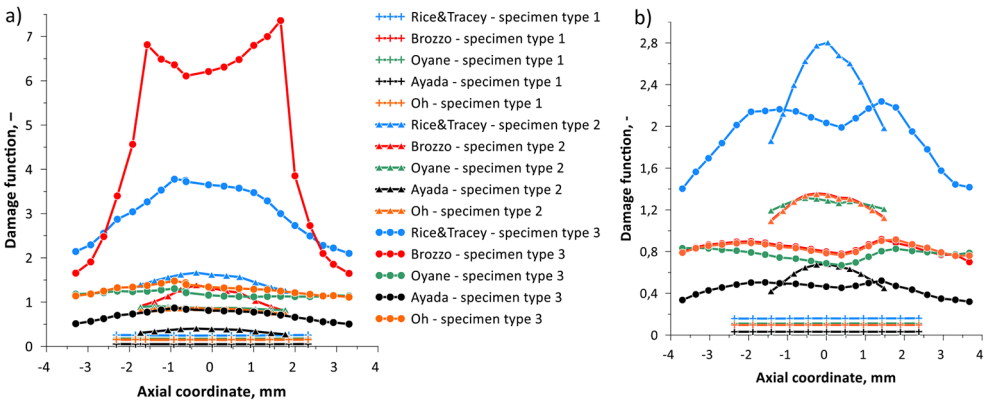

Figure 9. Distribution of dimensionless damage functions for: a) CW008A copper, b) S355 steel, in tensile test

the critical values of the damage function (Tables 5 and 6). To calculate the critical value according to Oyane's criterion, based on [7], the material constant was set to A = 0.424. The data presented in the tables below are average values obtained from individual sensors placed in the tested samples.

The analysis of the data presented in the tables shows that the value of the damage function depends on the material grade and the geometry of the specimens. The values of the stress functions of damage obtained in the tensile test for both tested materials are lower than those obtained in the torsion test. The main limitation of the method used is that the obtained critical values of the damage function for the tested ductile fracture criteria can only be applied to the case of shaping characterized by a similar stress state to that found in the tests studied.

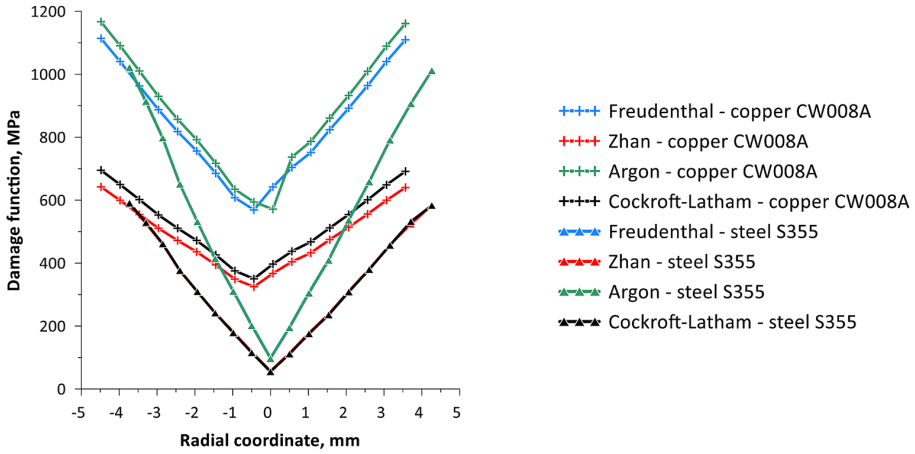

Figure 10. Distribution of stress damage functions for: a) CW008A copper, b) S355 steel, in the torsion test

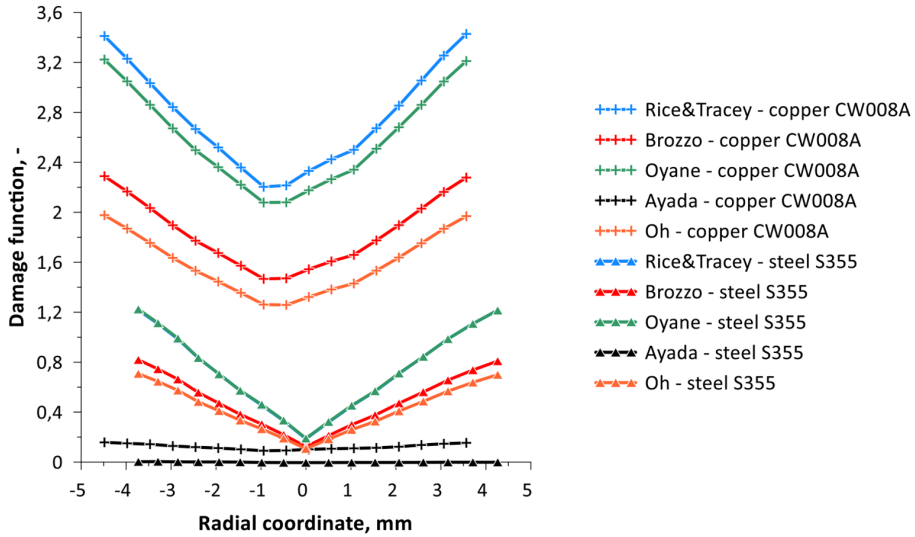

Figure 11. Distribution of dimensionless damage functions for: a) CW008A copper, b) S355 steel, in torsion test

Table 5. Critical values of the damage function for CW008A copper in tensile and torsion test, in the temperature of 293.15 K

Type	C_{FREU} [MPa]	C_{ZHAN} [MPa]	C_{ARGO} [MPa]	C_{CL} [MPa]	C_{RT}	C_{BROZ}	C_{OYAN}	C_{AYAD}	C_{OH}
Tensile, type 1	55.9	37.3	74.1	55.4	0.24	0.15	0.17	0.05	0.15
Tensile, type 2	271.7	178.8	424.9	332.1	1.6	1.3	0.86	0.39	0.85
Tensile, type 3	320.2	209.1	640.2	529.1	3.6	2.7	1.1	0.81	1.3
Torsion	1113.9	642.2	1166.8	695.1	3.4	2.3	3.2	0.16	1.9

Table 6. Critical values of the damage function for S355 steel in tensile and torsion test, in the temperature of 293.15 K

Type	C_{FREU} [MPa]	C_{ZHAN} [MPa]	C_{ARGO} [MPa]	C_{CL} [MPa]	C_{RT}	C_{BROZ}	C_{OYAN}	C_{AYAD}	C_{OH}
Tensile, type 1	68.0	45.3	90.6	67.9	0.16	0.1	0.1	0.03	0.1
Tensile, type 2	746.2	494.0	1255.5	1003.3	2.8	1.35	0.29	0.68	1.34
Tensile, type 3	363.7	238.1	707.6	582.1	2.03	0.8	0.69	0.46	0.78
Torsion	1018.7	587.9	1021.5	590.7	1.2	0.82	1.22	0.004	0.71

CONCULSIONS

The following conclusions have been drawn from the study. The critical values of the damage function can be determined by classical calibration tests – tensile and torsion tests. The values of stress and dimensionless damage functions for type 1 specimens subjected to tensile testing for both materials in the cross-section show a linear distribution; for the other types of specimens, the values of the damage functions took over their maximum values in the centre of the specimen – at the point of appearing necking. The values of the stress and dimensionless damage functions for specimens subjected to torsion testing for both materials show the lowest value at the point located in the centre of the specimen; these values increase with the approach to the lateral surfaces, where the damage functions show the highest values. The critical values of the damage function depend on the material grade and geometry of the specimens. The obtained results of the research allowed the determination of the limiting values of the damage functions for CW008A copper and S355 steel at a forming temperature of 293.15 K, which will make it possible to find the critical damage value of the investigated failure criterion for a given forming case. Further research is intended in the direction of determining the limits of the damage function for classical calibration tests, extending the research to different ranges of forming temperatures and available ductile fracture criteria.

REFERENCES

1. Wyrzykowski J.W., Pleszakow E., Sieniewski J. Odkształcenie i pękanie metali, Warszawa, Wydawnictwo Naukowo-Techniczne, 1999.
2. Pineau A., Beuzerga A.A., Pardoen T. Failure of metals I: brittle and ductile fracture, Acta Materialia, 2016; 107: 424–483.
3. Seaman L., Curvan D.R., Shockey D.A. Computational models for ductile and brittle fracture, Journal of Applied Physics 1976; 47: 4814–4826.
4. Argon A.S., Im J., Safoglu R. Cavity formation from inclusions in ductile fracture, Metallurgical Transactions A 1975; 6(4): 825–837.
5. Anderson T.L. Fracture mechanics. Fundamentals and Applications, Boca Raton, Taylor & Francis, 2005.
6. Lemaitre J., Dasmorat R. Engineering damage mechanics, ductile, creep and brittle failures, Berlin, Springer, 2005.
7. Kraišnik M., Vilotič D., Šidanin L., Stefanovič M. Various approaches to defining the criteria of ductile crack in cold bulk forming processes. International Journal of Engineering 2015; 13(2): 213–218.
8. Fischer F.D., Kolednik O., Shan G.X., Rammerstorfer F.G. A note on calibration of ductile failure damage indicators. International Journal of Fracture 1995; 73: 345–357.
9. Fuertes J.P., Luru R., Luis C.J., Salcedo D., Leon J., Puertas I. Comparative study of the damage attained with different specimens by FEM. Procedia Engineering 2015; 132: 319–325.
10. Kvačkaj T., Tiža J., Bascó J., Kováčová, Kočiško R., Pernis R., Fedorčáková M., Pures P., Cockcroft–Latham ductile fracture criteria for nonferrous materials. Materials Science Forum 2014; 782: 373–378.
11. Watanabe A., Fujikawa S., Ikeda A., Shiga N. Prediction of ductile fracture in cold forming, Procedia Engineering 2014; 81: 425–430.
12. Jia W., Ma L., Le Q., Zhi C., Liu P. Deformation and fracture behaviors of AZ31B Mg alloy at elevated temperature under uniaxial compression. Journal of Alloys and Compounds 2019; 783: 863–876.
13. Pater Z., Gontarz A. Critical damage values of R200 and 100Cr6 steels obtained by hot tensile testing. Materials 2019; 12(7): 1–12.